


RESEARCH ARTICLE

Regional vesicular acetylcholine transporter distribution in human brain: A [¹⁸F]fluoroethoxybenzovesamicol positron emission tomography study

Roger L. Albin^{1,2,3,4}  | Nicolaas I. Bohnen^{1,2,3,5} | Martijn L. T. M. Muller^{3,5} | William T. Dauer^{1,2,3,6} | Martin Sarter^{3,7} | Kirk A. Frey^{2,5} | Robert A. Koeppe^{3,5}

¹Neurology Service & GRECC, VAAHS, Ann Arbor, Michigan

²Department of Neurology, University of Michigan, Ann Arbor, Michigan

³University of Michigan Morris K. Udall Center of Excellence for Research in Parkinson's Disease, Ann Arbor, Michigan

⁴Michigan Alzheimer Disease Center, Ann Arbor, Michigan

⁵Department of Radiology, University of Michigan, Ann Arbor, Michigan

⁶Department of Cell and Developmental Biology, University of Michigan, Ann Arbor, Michigan

⁷Department of Psychology, University of Michigan, Ann Arbor, Michigan

Correspondence

Roger L. Albin, MD, 5023 BSRB, 109 Zina Pitcher Place, Ann Arbor, MI, 48109-2200, USA.

Email: ralbin@umich.edu

Funding information

Michael J. Fox Foundation for Parkinson's Research; NIH-NINDS, Grant/Award Number: P01 NS015655P50 NS091856R21 NS088302; Michael J. Fox Foundation

Abstract

Prior efforts to image cholinergic projections in human brain in vivo had significant technical limitations. We used the vesicular acetylcholine transporter (VChT) ligand [¹⁸F]fluoroethoxybenzovesamicol ([¹⁸F]FEOBV) and positron emission tomography to determine the regional distribution of VChT binding sites in normal human brain. We studied 29 subjects (mean age 47 [range 20–81] years; 18 men; 11 women). [¹⁸F]FEOBV binding was highest in striatum, intermediate in the amygdala, hippocampal formation, thalamus, rostral brainstem, some cerebellar regions, and lower in other regions. Neocortical [¹⁸F]FEOBV binding was inhomogeneous with relatively high binding in insula, BA24, BA25, BA27, BA28, BA34, BA35, pericentral cortex, and lowest in BA17–19. Thalamic [¹⁸F]FEOBV binding was inhomogeneous with greatest binding in the lateral geniculate nuclei and relatively high binding in medial and posterior thalamus. Cerebellar cortical [¹⁸F]FEOBV binding was high in vermis and flocculus, and lower in the lateral cortices. Brainstem [¹⁸F]FEOBV binding was most prominent at the mesopontine junction, likely associated with the pedunclopontine–laterodorsal tegmental complex. Significant [¹⁸F]FEOBV binding was present throughout the brainstem. Some regions, including the striatum, primary sensorimotor cortex, and anterior cingulate cortex exhibited age-related decreases in [¹⁸F]FEOBV binding. These results are consistent with prior studies of cholinergic projections in other species and prior postmortem human studies. There is a distinctive pattern of human neocortical VChAT expression. The patterns of thalamic and cerebellar cortical cholinergic terminal distribution are likely unique to humans. Normal aging is associated with regionally specific reductions in [¹⁸F]FEOBV binding in some cortical regions and the striatum.

KEYWORDS

acetylcholine, aging, basal forebrain, cerebellum, pedunclopontine nucleus, RRID: SCR_001847, RRID: SCR_007037, striatum, thalamus

Abbreviations: AC, anterior cingulate cortex; ACh, acetylcholine; AChase, acetylcholinesterase; AD, Alzheimer disease; AM, amygdala; BF, basal forebrain; ChAT, choline acetyltransferase; FEOBV, fluoroethoxybenzovesamicol; FL, flocculus; HIP, hippocampal formation; LG, lateral geniculate nucleus; MP, mesopontine; MP4A, N-methyl-4-piperidyl acetate; MVC, medial vestibular complex; PD, Parkinson disease; PET, positron emission tomography; PMP, methyl-4-piperidiny propionate; PPN-LDT, pedunclopontine–laterodorsal tegmental complex; SMC, sensorimotor cortex; SPECT, single photon emission computed tomography; SUVR, standardized uptake value ratio; THAL, thalamus; VChT, vesicular acetylcholine transporter; VER, vermis

1 | INTRODUCTION

Acetylcholine (ACh) is the primary neurotransmitter of several CNS neuron populations. These include neurons of the basal forebrain (BF) complex projecting to numerous cortical regions, striatal cholinergic interneurons, the medial habenula–interpeduncular nucleus projection, projections of the pedunclopontine–laterodorsal tegmental (PPN-LDT) complex, the parabrachial nucleus, some medial vestibular complex (MVC) neurons, and brainstem motor and autonomic

neurons. BF cholinergic pathways participate in the modulation of important cognitive functions such as attention and executive function (Ballinger, Ananth, Talmage, & Role, 2016; Hasselmo & Sarter, 2011; Prado, Janickova, Al-Onaizi, & Prado, 2017). Projections of the PPN-LDT complex may play important roles in the regulation of sleep and waking, and some data implicates these neurons in control of balance and gait (Gut & Winn, 2016; Mena-Segovia & Bolam, 2017; Pienaar, Vernon, & Winn, 2016). Striatal cholinergic interneurons are the subject of intense investigations and play important roles in the control of a variety of functions mediated by the striatal complex (Deffains & Bergman, 2015; Gonzales & Smith, 2015; Tanimura et al., 2017).

Abnormalities of some of these pathways are implicated in neurologic and psychiatric disease, particularly Alzheimer disease (AD), Parkinson disease (PD), and tobacco abuse. Degeneration of the BF complex is documented well in AD and PD, and degeneration of cholinergic PPN-LDT neurons may drive important aspects of declining gait and balance functions in PD and Progressive Supranuclear Palsy (Bohnen et al., 2012; Gilman et al., 2010; Hirsch, Graybiel, Duyckaerts, & Javoy-Agid, 1987; Mesulam, 2013; Mufson, Ginsberg, Ikonovic, & DeKosky, 2003; Schliebs & Arendt, 2011). Augmenting cholinergic neurotransmission with acetylcholinesterase inhibitors is an accepted treatment for dementias, including AD, Lewy body dementia, and PD-associated dementia. Anti-muscarinic cholinergic agents are used for the treatment of dystonias and for treatment of PD-associated tremor. Manipulations of cholinergic neurotransmission are being pursued to improve gait and balance functions in PD (Chung, Lobb, Nutt, & Horak, 2010; Henderson et al., 2016; Kucinski, De Jong, & Sarter, 2017; Li et al., 2015). Nicotinic cholinergic receptors mediate the addictive effects of nicotine and drugs active at this receptor family are used to treat nicotine addiction (Anthenelli et al., 2016). Improved understanding of the organization of cholinergic pathways in the human brain is relevant to efforts to expand useful cholinergic pharmacology in the treatment of human neurologic and psychiatric diseases.

Prior investigations in other species, including nonhuman primates, and work with postmortem human tissues provided considerable information about the organization of human brain cholinergic pathways (Albin, Morgan, Higgins, & Frey, 1994; Barmack, Baughman, & Eckenstein, 1992; Barmack, Baughman, Eckenstein, & Shojaku, 1992; de Lacalle et al., 1994; De Lacalle, Hersh, & Saper, 1993; Emre, Heckers, Mash, Geula, & Mesulam, 1993; Fitzpatrick, Diamond, & Raczkowski, 1989; Fukushima et al., 2001; Gilmor et al., 1996, 1999; Heckers, Geula, & Mesulam, 1992; Ichikawa, Ajiki, Matsuura, & Misawa, 1997; Jaarsma et al., 1997; Kus et al., 2003; Levey, Hallanger, & Wainer, 1987; Mahady, Perez, Emerich, Wahlberg, & Mufson, 2017; Manaye et al., 1999; Mesulam, 2004; Mesulam & Geula, 1988; Mesulam, Geula, Bothwell, & Hersh, 1989; Mesulam, Hersh, Mash, & Geula, 1992; Mesulam, Mash, Hersh, Bothwell, & Geula, 1992; Roghani, Shirzadi, Butcher, & Edwards, 1998; Schäfer, Eiden, & Weihe, 1998; Schaffer, Weihe, Erickson, & Eiden, 1995; Woolf, 1991; Woolf & Butcher, 1985, 1986, 1989; Woolf, Eckenstein, & Butcher, 1984; Zhang, Zhou, & Yuan, 2016). Working with postmortem tissues has intrinsic limitations and inferences from studies of other species may be confounded by inter-species differences.

To advance our understanding of the organization of cholinergic pathways in humans, we assessed the regional distribution of human brain cholinergic neuron terminals with [^{18}F]fluoroethoxybenzovesmicol ([^{18}F]FEOBV) positron emission tomography (PET; Aghourian et al., 2017; Petrou et al., 2014). FEOBV is a high-affinity ligand for the vesicular acetylcholine transporter (VACHT), the protein responsible for pumping ACh from the cytosol into synaptic vesicles (Prado et al., 2017; Prado, Roy, Kolisnyk, Gros, & Prado, 2013). VACHT is expressed at uniquely high levels by cholinergic neurons (Arvidsson, Riedel, Elde, & Meister, 1997). Prior human imaging studies of brain VACHT expression used less resolute single photon emission computed tomography (SPECT) methods (Kuhl et al., 1994, 1996; Lamare et al., 2013). Prior PET studies of regional cholinergic terminal distribution used acetylcholinesterase (AChase) substrates ([^{11}C]methyl-4-piperidyl propionate [PMP]; N-[^{11}C]methyl-4-piperidyl acetate [MP4A]) to identify cholinergic synapses (Iyo et al., 1997; Kuhl et al., 1999). These methods are less specific. AChase, for example, is produced by midbrain dopaminergic neurons and high regional AChase activity was detected in regions, the lateral cerebellar cortices, not suspected to have substantial cholinergic terminal innervation (Greenfield, 1991; Kuhl et al., 1999). AChase enzyme activity may be regulated by synaptic activity and disease states, a potential obstacle to quantifying regional cholinergic terminal density (DeKosky et al., 1992). The very high AChase expression characteristic of the striatum limits quantification of striatal AChase as PMP and MP4A metabolite accumulation may be flow, rather than AChase activity, limited. PMP and MP4A are also, though to a considerably lesser extent, butyrylcholinesterase substrates and butyrylcholinesterase activity changes might influence the results of PET studies with these tracers (Snyder et al., 2001).

We describe the regional distribution of [^{18}F]FEOBV binding in human volunteers with no evidence of neurologic or psychiatric disease. Our results largely confirm inferences from postmortem human studies and nonhuman mammal studies but indicate distinctive features of human cholinergic pathways and indicate effects of aging.

2 | METHODS

2.1 | Subjects

We studied 29 subjects without histories of the neurologic or psychiatric disease. We studied 18 men and 11 women. The mean age was 47 years ($SD = 21$ years); age range 20–81 years. No subject was using a medication that might affect cholinergic neurotransmission and none were using tobacco or nicotine products. Informed consent was obtained from all subjects prior to study entry and this study was approved by the University of Michigan Medical School IRB. Limited results were reported previously from subsets of these subjects (Albin, Minderovic, & Koeppe, 2017; Petrou et al., 2014).

2.2 | [^{18}F]FEOBV PET

[^{18}F]FEOBV was prepared as described previously (Petrou et al., 2014; Shao et al., 2011). [^{18}F]FEOBV (288–318 MBq) was

administered via intravenous bolus. Twenty-eight subjects were scanned on an ECAT Exact HR+ PET tomograph (Siemens Molecular Imaging, Knoxville, TN). One subject was scanned on a Biograph True-Point scanner (Model 1094; Siemens Molecular Imaging). Brain imaging was conducted in three imaging periods. The first period began at injection and continued for 90 min. The subjects were then given a 30-min break, followed by a second imaging period from 120 to 150 min, an additional break, and then a third imaging period from 180 to 210 min. Dynamic PET scans were reconstructed using Fourier rebinning (FORE) and the iterative 2D-OSEM algorithm, with four iterations, 16 subsets, and no postreconstruction smoothing. The entire dynamic sequence was co-registered to the final form of the first 90-min scanning period. The first seven studies were acquired with a slightly different protocol, where the first scanning period last for 120 min, and the second and third periods lasted from 150 to 180 and 210 to 240 min, respectively.

2.3 | MRI

MRI imaging was performed on a 3 Tesla Philips Ingenia System (Philips) using a 15-channel head coil. A standard T1 weighted series of a 3D inversion recovery prepared turbo-field echo was performed in the sagittal plane using TR/TE/TI = 9.8/4.6/1041 ms; turbo factor = 200; single average; FOV = 240 × 200 × 160 mm; acquired matrix = 240 × 200. One hundred and sixty slices were reconstructed to 1-mm isotropic resolution.

2.4 | Analysis of [¹⁸F]FEOBV binding

The primary analysis was performed using the average of the co-registered 180–210 min scan period (termed “late static”). For the seven scans that had a slightly different acquisition sequence, we used the average of both the 150–180 and 210–240 time windows, thus matching the median of the scan data used of 195 min. FreeSurfer (freesurfer-i386-apple-darwin11.4.2-stable6-20170119; <https://surfer.nmr.mgh.harvard.edu/fswiki/FreeSurferMethodsCitation>; RRID: SCR_001847) was used on each individual's T1-weighted MR to define gray matter and white matter voxels. The entire co-registered PET sequence was registered to the MR. The segmented white matter mask from FreeSurfer (1 for WM; 0 elsewhere) was smoothed to PET resolution, and then a threshold of 0.90 applied to the mask, yielding a volume of interest where the partial volume contribution from nonwhite matter regions to the mask was <10% for every voxel. This white matter volume-of-interest was then applied to the PET data and used as a normalizing (intensity scaling) factor for the late static scan. Accordingly, [¹⁸F]FEOBV binding in each volume of interest was expressed as standardized uptake value ratios (SUVs). We showed previously that this approach is equivalent to kinetic modeling approaches for quantifying regional brain [¹⁸F]FEOBV binding (Albin et al., 2017).

We used NeuroStat (<https://neurostat.neuro.utah.edu/>) and Statistical Parametric Mapping (SPM12; <http://www.fil.ion.ucl.ac.uk/spm/>; RRID: SCR_007037) to nonlinearly warp all PET scans into the Talairach and International Consortium for Brain Mapping atlas spaces, respectively. This was done to allow the creation of mean images of all subjects, plus mean images for young and elderly cohorts, and to allow

better visualization of effects of aging. We also used our standard VOI set developed for Talairach space, which is based entirely on the PET scans (no MR), as described previously (Bohnen et al., 2006). Brainstem parcellation was performed as described previously (Albin et al., 2008). To complement this regional analysis, cortical and subcortical segmentation was performed with FreeSurfer. The programs were run in the fully automated mode. Volumes for all FreeSurfer-defined brain structures were obtained as part of the standard FreeSurfer output. The VOIs were then applied in native MR-space to the co-registered PET scans. Results were essentially identical to those of the Neurostat-SPM based analysis and are not shown.

To analyze thalamic [¹⁸F]FEOBV binding, we used the FreeSurfer-defined thalami, assumed an ellipsoid volume, and estimated the long axis of the ellipsoid volume. We then divided each hemisphere of the thalamus into octants, based on voxels medial versus lateral, anterior versus posterior, and superior versus inferior to the axis.

2.5 | Aging effects

To assess potential aging effects, we took advantage of the fact that our study population was divided into two groups; a younger group ($N = 13$; Mean 25 years; range 20–38) and an older group ($N = 16$; Mean 66 years; range 52–81). Inspection of averaged images for these groups suggested regionally specific age-related declines in [¹⁸F]FEOBV binding accompanying aging. Selected regions exhibiting possible age-related declines were compared with regions that appeared unchanged with aging. Examined regions included the striatal complex, thalamus, primary sensorimotor cortex (BAs 1–35), anterior cingulate cortex (BAs 24,32), hippocampal formation, amygdala, posterior cingulate cortex (BAs 23,31), cerebellar vermis, occipital cortex (BAs 17–19), lateral frontal cortex (BAs 44–47), and medial frontal cortex (BAs 8–10).

2.6 | Statistical analysis

[¹⁸F]FEOBV binding was compared within some regions using standard parametric methods. Analyses are described in each relevant Results section.

3 | RESULTS

3.1 | Overall

Brain [¹⁸F]FEOBV binding was distributed inhomogeneously (Figure 1; Table 1). Binding was highest in the striatal complex, followed by portions of the thalamus, amygdala and hippocampal formation, some neocortical regions, rostral brainstem, and some regions of the cerebellar cortex. The overall distribution and regional density of [¹⁸F]FEOBV binding is largely consistent with the distribution of cholinergic terminals described in prior human postmortem and nonhuman mammal studies (Albin et al., 1994; Barmack, Baughman, & Eckenstein, 1992; Barmack, Baughman, Eckenstein, & Shojaku, 1992; de Lacalle et al., 1993, 1994; Emre et al., 1993; Fitzpatrick et al., 1989; Fukushima et al., 2001; Gilmor et al., 1996, 1999; Heckers et al., 1992; Ichikawa et al., 1997; Jaarsma et al., 1997; Levey et al., 1987;

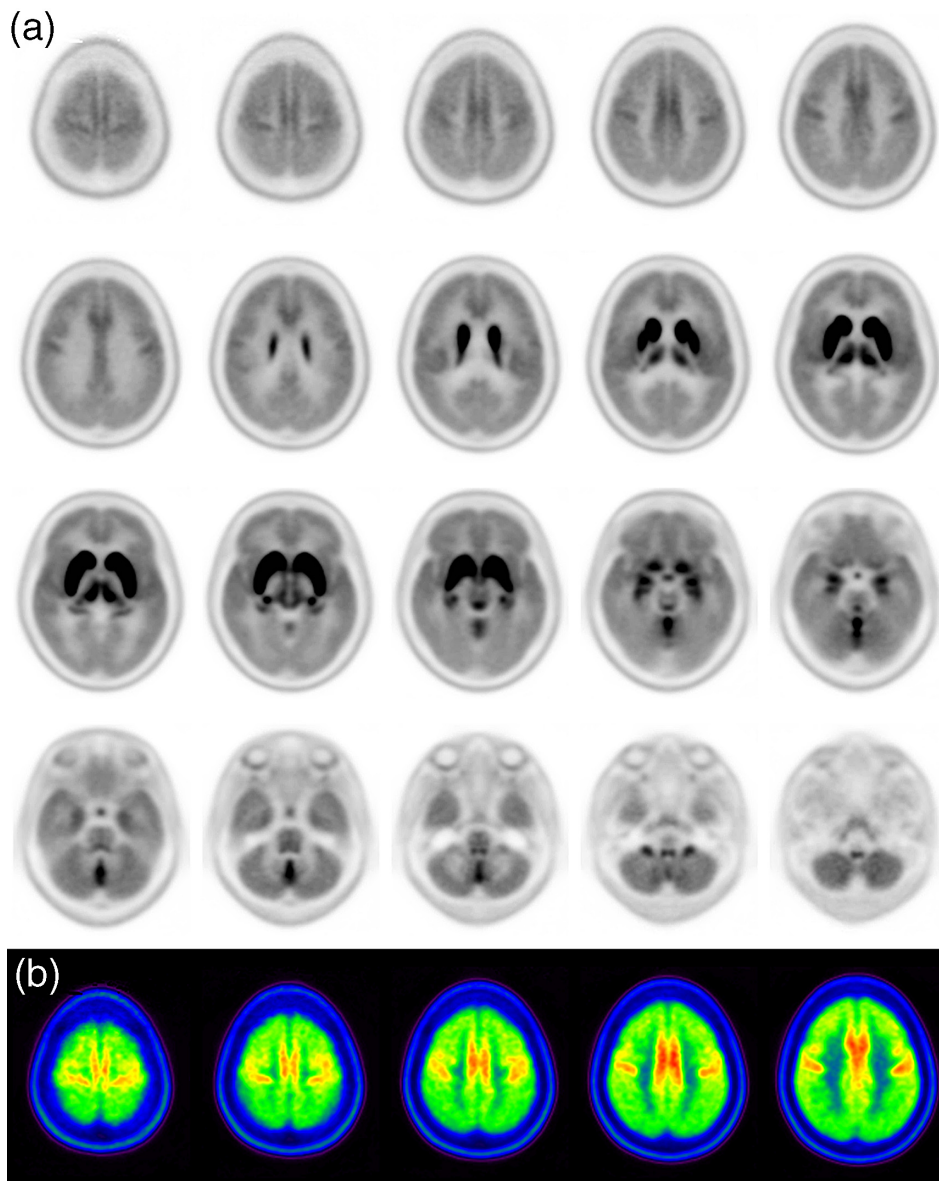


FIGURE 1 $[^{18}\text{F}]$ FEOBV binding in human brain. (a) Dorsal to ventral survey of averaged transaxial images for all 29 subjects. Images scaled to peak SUVR of 3.0. Regions with notable $[^{18}\text{F}]$ FEOBV binding include the striatal complex, thalamus, amygdala, hippocampal formation, neocortical mantle, mesopontine junction, and portions of the cerebellum (see text for details). (b) Pseudocolor images of dorsal transaxial levels (identical to top row in [a] above) to illustrate differing $[^{18}\text{F}]$ FEOBV binding in different cortical regions. Scaled to peak SUVR of 2.5. These images demonstrate relatively higher $[^{18}\text{F}]$ FEOBV binding in primary sensorimotor and anterior cingulate cortices

Mahady et al., 2017; Manaye et al., 1999; Mesulam, 2004; Mesulam et al., 1989; Mesulam & Geula, 1988; Mesulam, Hersh, et al., 1992; Mesulam, Mash, et al., 1992; Roghani et al., 1998; Schafer et al., 1995; Schäfer et al., 1998; Woolf, 1991; Woolf et al., 1984; Woolf & Butcher, 1985, 1986, 1989; Zhang et al., 2016). Our results are consistent as well with prior VAcHT ligand human SPECT imaging studies (Kuhl et al., 1994, 1996; Lamare et al., 2013).

Our results likely identify the distribution of and quantify the regional density of major cholinergic terminal systems in the human brain; cholinergic projections originating in the BF, striatal cholinergic interneurons, ascending and descending projections from the PPN/LDT complex, and cholinergic MVC projection neurons. It was not possible to clearly identify cholinergic nuclei or terminals associated with the

medial habenular–interpeduncular nucleus projection or the parabigeminal nucleus to collicular projection, though the parabigeminal nucleus may be included in a region of relatively high $[^{18}\text{F}]$ FEOBV binding at the mesopontine junction (see below). It was not possible to identify brainstem motor or autonomic cholinergic nuclei. More detailed description of the identifiable projections–regions follows.

3.2 | Striatal complex

Consistent with the known very high expression of cholinergic markers in the striatal complex, striatal complex $[^{18}\text{F}]$ FEOBV binding was the highest of all brain regions, well above levels expressed in any other region. Striatal complex $[^{18}\text{F}]$ FEOBV binding was mildly

TABLE 1 Bilaterally averaged [¹⁸F]FEOBV binding within selected volumes of interest

Region	Mean SUVR	SD	Region	Mean SUVR	SD
BA1	1.80	0.19	BA43	1.84	0.18
BA2	1.77	0.17	BA44	1.78	0.14
BA3	1.84	0.20	BA45	1.70	0.15
BA4	1.92	0.23	BA46	1.68	0.15
BA5	1.74	0.19	BA47	1.81	0.15
BA6	1.87	0.19	Amygdala	3.14	0.39
BA7	1.60	0.13	Hippocampal formation	2.76	0.31
BA8	1.66	0.14	Insula	2.57	0.29
BA9	1.71	0.13	Caudate	7.67	1.31
BA10	1.69	0.14	Dorsal caudate	8.00	1.41
BA11	1.67	0.14	Ventral striatum	7.00	1.29
BA12	1.82	0.18	Putamen	8.89	1.43
BA17	1.53	0.15	Anterior putamen	9.01	1.47
BA18	1.48	0.12	Posterior putamen	8.53	1.40
BA19	1.52	0.12	Thalamus	3.45	0.57
BA20	1.65	0.16	Lateral geniculate nucleus	3.47	0.60
BA21	1.73	0.15	Cerebellar hemisphere cortex	1.80	0.16
BA22	1.89	0.17	Cerebellar vermis cortex	3.08	0.38
BA23	1.68	0.14	Flocculus	2.22	0.33
BA24	2.12	0.23	Midbrain	2.35	0.28
BA25	2.89	0.63	Substantia Nigra	2.01	0.27
BA26	1.87	0.27	Raphe nucleus	2.61	0.41
BA27	2.37	0.57	Dorsal midbrain	2.85	0.30
BA28	2.50	0.39	Pons	2.09	0.25
BA29	1.45	0.14	Rostral pons	2.35	0.28
BA30	1.65	0.23	Caudal Pons and Medulla	2.38	0.25
BA31	1.75	0.14	Medulla	2.05	0.28
BA32	2.01	0.20			
BA34	2.71	0.40			
BA35	2.20	0.35			

heterogeneous. [¹⁸F]FEOBV binding was highest in the putamen and lower in the caudate nucleus (Table 1; paired *t* test, $p < .0001$). The striatal complex was further subdivided in dorsal caudate, ventral striatum (nucleus accumbens and ventral caudate), anterior putamen, and posterior putamen (Table 1). [¹⁸F]FEOBV binding was modestly different in all these subregions (one-way ANOVA for correlated samples, $p < .0001$; all subregions different from each other, Tukey's HSD, $p < .01$). The rank order of striatal complex [¹⁸F]FEOBV binding was Anterior Putamen > Posterior Putamen > Dorsal Caudate > Ventral Striatum.

3.3 | Cortex

[¹⁸F]FEOBV binding was distributed widely and somewhat inhomogeneously throughout the cortex. Most neocortical regions (BA1–23, 26, 29–32, 36–47; Figures 1 and 2) exhibited modest [¹⁸F]FEOBV binding (mean SUVRs = 1.5–2.0 range; Table 1) with some regions (BA24, 25, 27, 28, 34, and 35) exhibiting higher levels of [¹⁸F]FEOBV binding (mean SUVRs = 2.0–2.5 range; Table 1). Consistent with the results of the Brodmann areas based analysis, primary sensorimotor and anterior cingulate cortices were readily distinguished from

surrounding cortices (Figures 1 and 2). Similarly, there was a modest anterior to posterior gradient with frontal cortices exhibiting modestly higher levels of [¹⁸F]FEOBV binding than occipital cortices (Figures 1 and 2). Insular cortex was slightly higher (mean SUVR = 2.57; Table 1). As expected, the hippocampal formation (mean SUVR = 2.76) and amygdala (mean SUVR = 3.14) exhibited the highest [¹⁸F]FEOBV binding of any cortical region (Table 1, Figure 3).

3.4 | Thalamus

The thalamus exhibited relatively high but likely inhomogeneous [¹⁸F]FEOBV binding (Table 1, Figures 1 and 4). Grossly, thalamic [¹⁸F]FEOBV binding distribution did not exhibit the expected ovoid shape (Figures 1 and 4). In particular, the anterolateral border of thalamic [¹⁸F]FEOBV binding had a concave shape, suggesting less [¹⁸F]FEOBV binding in the anterolateral thalamus. In addition, the lateral geniculate nuclei exhibited high [¹⁸F]FEOBV binding and could be easily distinguished from the rest of the thalamus (Table 1, Figure 4). This suggests that portions of the thalamus more rostral and dorsal to the lateral geniculate nucleus, for example, portions of the pulvinar complex, had less [¹⁸F]FEOBV binding. In the absence of an established

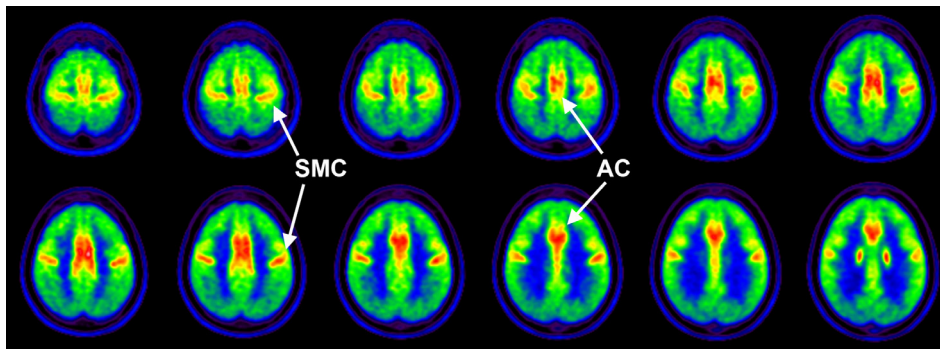


FIGURE 2 Neocortical [^{18}F]FEOBV binding. Transaxial images from near the vertex to the level of the striatum. Images scaled to emphasize differences in cortical regions. Consistent with Brodmann area based analysis (Table 1; see text), higher [^{18}F]FEOBV binding in primary sensorimotor (SMC) and anterior cingulate (AC) cortices. There is a modest anterior to posterior gradient with higher frontal cortical than occipital cortical [^{18}F]FEOBV binding

parcellation of the thalamus, we divided the thalamus into eight subregions by assuming that the thalamus has ovoid shape with a major rostral-caudal axis, excluding the lateral geniculate nuclei (see section 2). In general, consistent with the impression that anterolateral regions exhibited less [^{18}F]FEOBV binding, the lateral subregions defined by this analysis had less [^{18}F]FEOBV binding than medial subregions and anterior subregions had less [^{18}F]FEOBV binding than posterior regions (Table 2). This was confirmed by statistical comparisons of cognate octants (e.g., superior anterolateral octant vs. superior anteromedial octant; superior anterolateral octant vs. superior posterolateral octant, etc.). All medial octants had significantly higher [^{18}F]FEOBV binding than cognate lateral octants and all posterior octants had significantly higher [^{18}F]FEOBV binding than cognate anterior octants ($p < 0.05$; paired t tests with Bonferroni correction for multiple comparisons). This approach may not sample the pulvinar complex adequately. As seen in Figure 4B, the lateral geniculate nuclei appear relatively isolated, suggesting that the pulvinar complex, rostral and dorsal to the lateral geniculate, exhibits relatively low [^{18}F]FEOBV binding.

3.5 | Cerebellum

All regions of cerebellar cortex exhibited [^{18}F]FEOBV binding with some regions exhibiting relatively high [^{18}F]FEOBV binding levels (Table 1, Figures 1 and 5). Highest cerebellar cortical [^{18}F]FEOBV binding was found in the vermis (mean SUVR = 3.1) with the cerebellar hemisphere cortices at significantly lower levels (mean SUVR = 1.8). The floccular region exhibited intermediate levels of [^{18}F]FEOBV binding (mean SUVR = 2.2).

3.6 | Brainstem

Significant [^{18}F]FEOBV binding (mean SUVRs in the 2–2.5 range) was present in all regions quantified (Table 1). Precise parcellation of the brainstem is very limited due to the small size of brainstem structures such as PPN-LDT complex and cranial nerve nuclei. [^{18}F]FEOBV binding was particularly concentrated in dorsal brainstem from the caudal midbrain to the mid pons (Figures 1 and 6). While difficult to quantify, there also appeared to be modestly increased [^{18}F]FEOBV binding in

the dorsal regions of the caudal brainstem, possibly within the periaqueductal tegmentum (Figures 1 and 6).

3.7 | Aging effects

Potential aging effects were assessed initially by comparing younger (22–38 years) and older (52–81 years) subjects. These comparisons revealed regionally specific changes accompanying aging (Table 3, Figures 7 and 8). Statistical significance of age-related changes was assessed with one-way independent t tests using the Holm-Bonferroni method to correct for multiple comparisons at a threshold of $p < .05$. Significant age-related changes were found in the striatum, primary sensorimotor cortex, and anterior cingulate cortex with trends

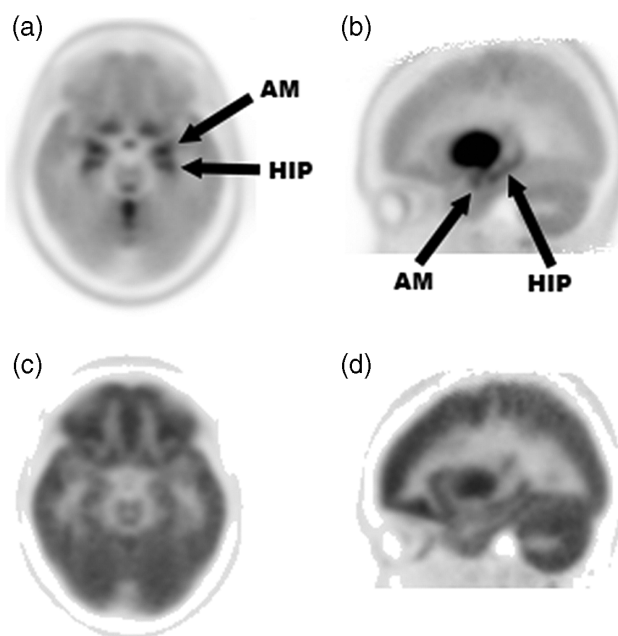


FIGURE 3 [^{18}F]FEOBV binding in amygdala and hippocampal formation. (a,b) [^{18}F]FEOBV binding. (a) Transaxial averaged image of all 29 subjects at level of anterior temporal lobe. (b) Parasagittal averaged image of all 29 subjects at level of amygdala (AM) and hippocampal formation (HIP). (c,d) early phase averaged images, representing the relative regional blood–brain ligand transport rate—Regional anatomy. (a,b) show significant [^{18}F]FEOBV binding and easily distinguishable amygdala and hippocampal formation

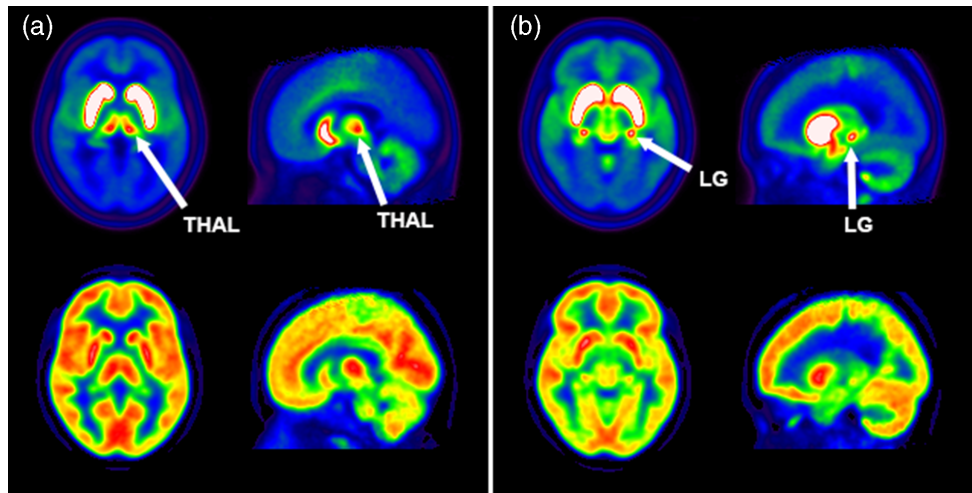


FIGURE 4 Thalamic [¹⁸F]FEOBV binding. Pseudocolor images of [¹⁸F]FEOBV binding (top row) and relative regional blood–brain ligand transport rate—Regional anatomy (bottom row). (a) Transaxial and parasagittal images at levels of dorsal thalamus (THAL). Note the inverted comma shape of high density of [¹⁸F]FEOBV binding in thalamus in the transaxial image compared with the ovoid shape of the thalamus in the transaxial flow image. (b) Transaxial and parasagittal images at levels of the lateral geniculate nuclei (LG). Note the relative isolation of high [¹⁸F]FEOBV binding in the lateral geniculate nuclei compared with surrounding regions, particularly the more anterior and dorsal pulvinar complex

TABLE 2 Bilaterally averaged thalamic octant SUVRs

Octant	Mean SUVR	SD
Superior anterior lateral	2.82	0.57
Superior anterior medial	3.15	0.55
Superior posterior lateral	3.40	0.71
Superior posterior medial	3.53	0.70
Inferior anterior lateral	2.79	0.53
Inferior anterior medial	3.61	0.48
Inferior posterior lateral	3.28	0.74
Inferior posterior medial	4.09	0.61

towards age-related declines in the thalamus, hippocampal formation, amygdala, and posterior cingulate (Table 3). There was no evidence of age-related decline in the cerebellar vermis and other cortical regions (Table 3). To further explore the relationship between aging and regional [¹⁸F]FEOBV binding, age was regressed against [¹⁸F]FEOBV binding in selected regions (Pearson product–moment correlations; Figure 8). Strong negative correlations were present in striatum

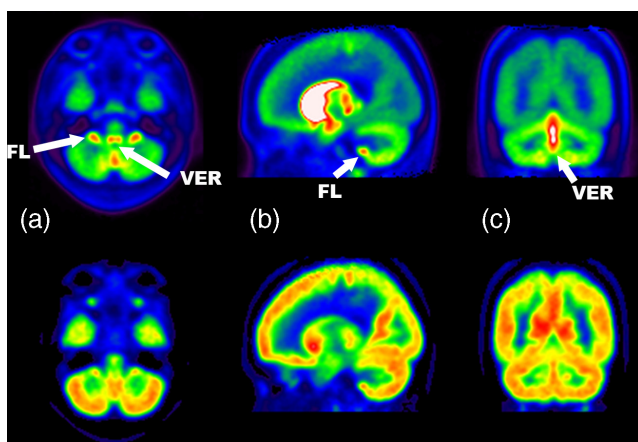


FIGURE 5 Cerebellar [¹⁸F]FEOBV binding. Pseudocolor images of [¹⁸F]FEOBV binding (top row) and relative regional blood–brain ligand transport rate—Regional anatomy (bottom row). (a) Transaxial images at the level of flocculi (FL). Note relatively high [¹⁸F]FEOBV binding in the floccular region, anterior vermis (VER), and posterior vermis (VER) with less [¹⁸F]FEOBV binding in the cerebellar hemispheres. (b) Parasagittal images at the level of the flocculus. (c) Coronal images at the level of the vermis. Again, note relatively high [¹⁸F]FEOBV binding in the vermis compared with the cerebellar hemispheres

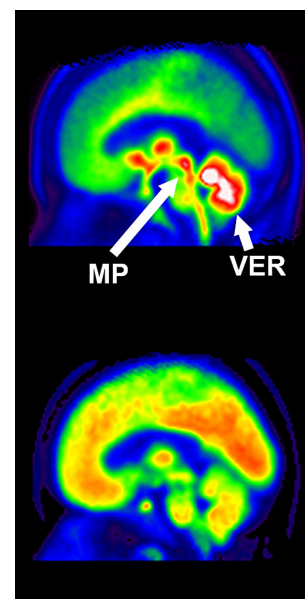
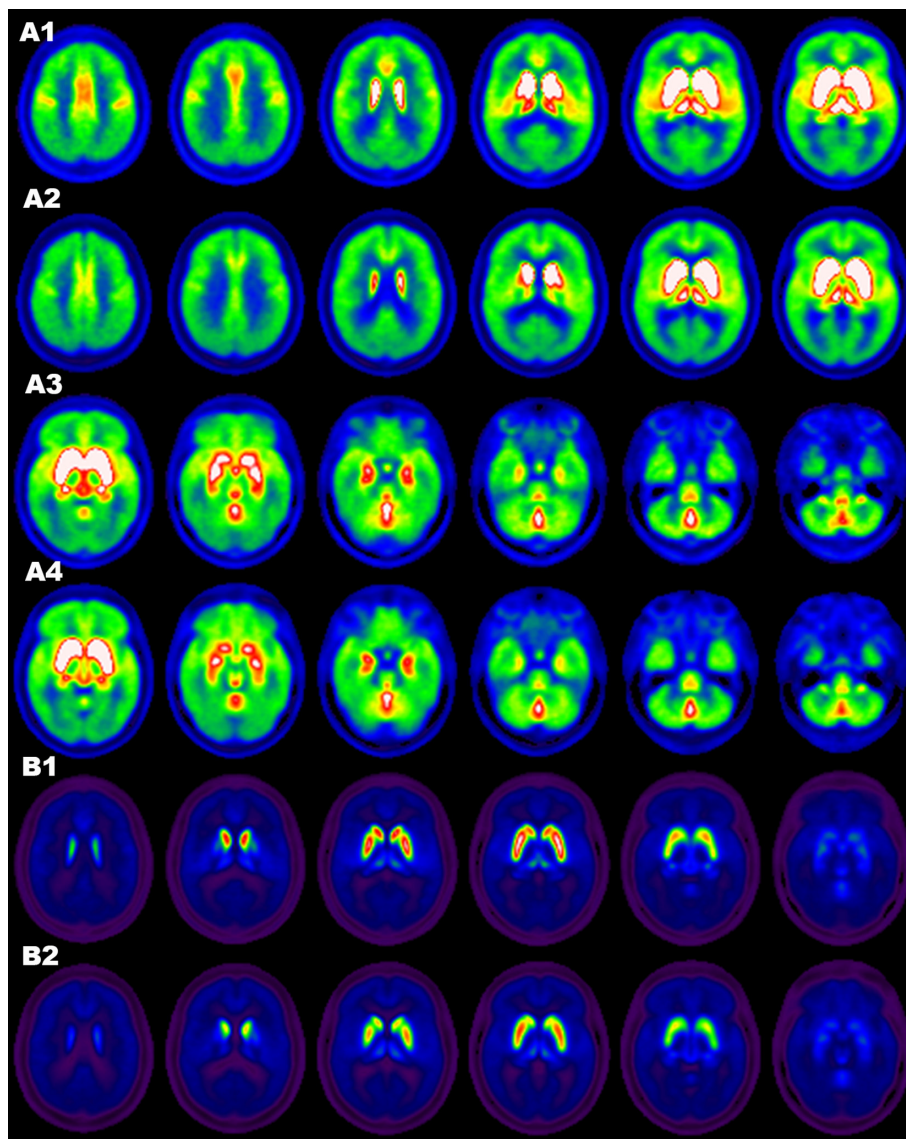


FIGURE 6 Brainstem [¹⁸F]FEOBV binding. Pseudocolor parasagittal images of [¹⁸F]FEOBV binding (top) and relative regional blood–brain ligand transport rate—Regional anatomy (bottom) in the midline plane. Relatively high [¹⁸F]FEOBV binding in the dorsal midbrain and spanning the mesopontine junction into rostral pons (MP). Increased [¹⁸F]FEOBV binding within the more dorsal caudal brainstem, possibly around the aqueduct

TABLE 3 Age-related regional changes in [¹⁸F]FEOBV binding. Values are SUVRs

Region	Young subject mean (SD)	Older subject mean (SD)	p
Striatal complex	9.16 (1.12)	7.39 (0.96)	<.0001*
Primary sensorimotor cortex	1.92 (0.15)	1.73 (0.96)	.002*
Anterior cingulate cortex	2.18 (0.16)	1.97 (0.20)	.0023*
Thalamus	3.68 (0.43)	3.26 (0.61)	.024
Hippocampal formation	2.89 (0.32)	2.66 (0.28)	.026
Posterior cingulate cortex	1.76 (0.11)	1.68 (0.14)	.062
Amygdala	3.26 (0.36)	3.05 (0.40)	.071
Cerebellar vermis	3.16 (0.49)	3.02 (0.26)	.165
Occipital cortex	1.52 (0.08)	1.50 (0.15)	.325
Medial frontal cortex	1.69 (0.08)	1.66 (0.16)	.280
Lateral frontal cortex	1.76 (0.08)	1.73 (0.17)	.300

*Significant after Holm–Bonferroni correction.

**FIGURE 7** Effects of aging on [¹⁸F]FEOBV binding. (a) Averaged transaxial pseudocolor images scaled at a peak of 10.0. a1 and a3—Young normal subjects. a2 and a4—Older normal subjects. Note declines in [¹⁸F]FEOBV binding in primary sensorimotor and anterior cingulate cortices in older normal subjects. (B) Averaged transaxial pseudocolor images scaled at a peak of 3.0 and at the levels of the striatal complex. b1—Young normal subjects. b2—Older normal subjects. Note decline in striatal complex [¹⁸F]FEOBV binding in older subjects

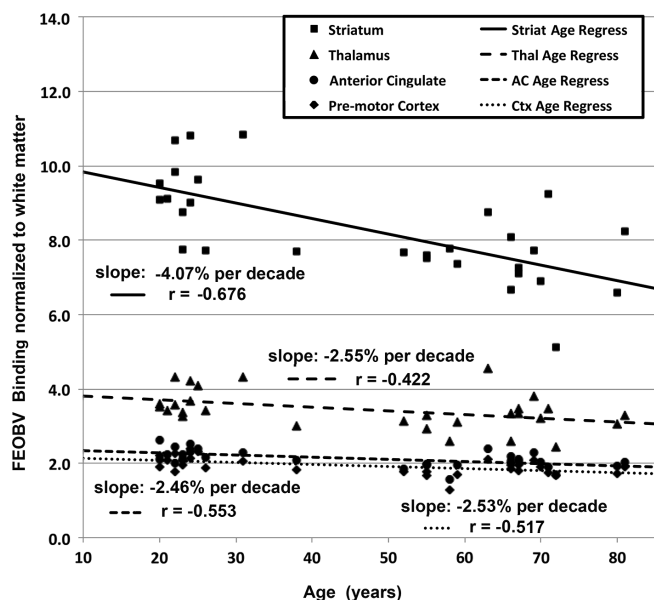


FIGURE 8 Correlations between age and regional [^{18}F]FEOBV binding. Pearson product-moment correlations between subject age and regional [^{18}F]FEOBV binding in striatum, primary sensorimotor cortex, anterior cingulate cortex, and thalamus. All correlations significant after Bonferroni correction at a threshold of 0.05

($r = .68$; $p < .00003$; decline of $\sim 4\%$ per decade), primary sensorimotor cortex ($r = .52$; $p < .003$; decline of $\sim 2.5\%$ per decade), and anterior cingulate cortex ($r = .55$; $p < .001$; decline of $\sim 2.5\%$ per decade), and thalamus ($r = 0.42$; $p < .0125$; decline of $\sim 2.5\%$ per decade). All correlations significant after Bonferroni correction at a threshold of 0.05. An interesting example of regionally specific decrease in [^{18}F]FEOBV binding was found in the primary sensorimotor cortex. In younger subjects, this region was easily distinguished from surrounding cortices by higher [^{18}F]FEOBV binding (Figure 7). In older subjects, primary sensorimotor cortex [^{18}F]FEOBV binding appeared more similar to surrounding cortices (Figure 7).

4 | DISCUSSION

VAcHT is thought to be uniquely expressed by cholinergic neurons. The VAcHT gene is part of a distinctive cholinergic “operon,” encoded within the first exon of the Choline Acetyltransferase gene (Eiden, 1998). FEOBV is a high affinity and specific ligand for VAcHT (Mulholland et al., 1998). In general, our findings correlate well with prior studies of brain cholinergic systems in humans and other mammals based on ChAT and high-affinity choline transporter immunohistochemistry (Kus et al., 2003; and see below). Our results also correlate well with nonhuman animal and limited human studies of the distribution of brain VAcHT immunoreactivity (Arvidsson et al., 1997; Gilmor et al., 1996, 1999; Ichikawa et al., 1997; Roghani et al., 1998; Schafer et al., 1995; Schäfer et al., 1998). Our results also correspond very well with prior limited human PET imaging with [^{18}F]FEOBV (Aghourian et al., 2017; Albin et al., 2017; Petrou et al., 2014).

4.1 | Striatal complex

The striatal complex exhibited the highest regional [^{18}F]FEOBV binding, indicating a very high density of cholinergic terminals within the

striatal complex. This result is consistent with a large body of data from studies in many species indicating uniquely high expression of cholinergic system markers and terminals in the striatal complex. There are at least two, and possibly three, sources of striatal cholinergic terminals. While striatal cholinergic interneurons comprise only a small fraction ($\sim 2\text{--}3\%$) of the total striatal neuron population (Bernácer, Prensa, & Giménez-Amaya, 2007; Gonzales & Smith, 2015; Lecumberri, Lopez-Janeiro, Corral-Domenge, & Bernacer, 2018) they give rise to dense axonal-terminal arborizations and play an important role in the integration of cortico- and thalamo-striate inputs with dopaminergic functions. The striatal complex also receives innervation from mesopontine (PPN-LDT) cholinergic neurons (Dautan et al., 2014; Dautan, Hacıoğlu Bay, Bolam, Gerdjikov, & Mena-Segovia, 2016; Woolf, 1991), presumably collaterals of neurons innervating the thalamus and other targets of the PPN-LDT complex. Mesulam, Hersh, et al. (1992) suggested that the human striatal complex receives some cholinergic afferents from the basal forebrain complex, a projection that is absent in rodents (Dautan et al., 2016). The relative proportion of striatal cholinergic interneuron terminals and extrinsic afferent terminals is unknown. It is generally assumed that striatal cholinergic interneuron terminals are much more abundant than extrinsic cholinergic afferent terminals. Janickova et al. (2017) genetically ablated VAcHT in murine PPN-LDT neurons. As measured by western immunoblots, VAcHT protein expression diminished markedly in the brainstem and thalamus and was unchanged in hippocampal formation, neocortex, and striatum. Genetic or toxic ablation of striatal cholinergic interneurons results in marked reductions in striatal cholinergic terminal markers (Aoki, Liu, Zucca, Zucca, & Wickens, 2015; Laplante, Lappi, & Sullivan, 2011; Martos, Braz, Beccaria, Murer, & Belforte, 2017; Pappas et al., 2015). These results are consistent with the traditional view that striatal extrinsic cholinergic afferents contribute only modestly to the total density of striatal cholinergic terminals. This is not to say that extrinsic cholinergic striatal afferents are functionally unimportant.

Our data suggest modest inhomogeneity of striatal cholinergic terminal density. [^{18}F]FEOBV binding was higher in the putamen than the caudate. Further subdividing these regions, we found highest [^{18}F]FEOBV binding within in the anterior putamen and lowest in the ventral striatum. In a stereological analysis of human postmortem material, Bernácer et al. (2007) described the inhomogeneous distribution of striatal cholinergic interneuron perikarya with higher density in the caudate nucleus than putamen. This is somewhat discordant with our results. While their definition of subregions is somewhat different from ours, their definition of caudate and putamen approximate our definition of dorsal caudate nucleus and putamen. The differences between our results and those of Bernácer et al. (2007) cautions against simple equation of perikaryal density and terminal density. Mesulam, Mash, et al. (1992) suggested that human cholinergic basal forebrain projections to the striatal complex more heavily innervate the putamen.

4.2 | Cortex

The cortical mantle receives its cholinergic inputs from cholinergic neurons of the basal forebrain complex (Ch1–Ch4 in the

nomenclature of Mesulam, Mufson, Wainer, & Levey, 1983). These cholinergic projections are known to participate in several important cognitive processes including attention, executive functions, and forms of memory (Ballinger et al., 2016; Hasselmo & Sarter, 2011; Prado et al., 2017). Our results are broadly consistent with data from older analyses of cholinergic terminal markers in human postmortem specimens (de Lacalle et al., 1994; Emre et al., 1993; Mesulam, 2004, 2013; Mesulam & Geula, 1988; Mesulam, Hersh, et al., 1992). Consistent with these prior descriptions, highest [^{18}F]FEOBV binding was found in amygdala and hippocampal formation, followed by paralimbic cortices, including the insular cortex, perirhinal cortex (BA35), entorhinal cortex (BA34, BA28), parahippocampal gyrus (BA27), and portions of the cingulate cortex (BA25, BA24). Regional binding density is probably not the only important difference in cholinergic innervation between cortical regions. Mesulam, Hersh, et al. (1992) also described varying laminar distributions of cholinergic terminals between neocortical regions. Detecting such differences is beyond the resolution of PET imaging. Similarly, prior studies indicate that the basolateral amygdala exhibits the highest density of cholinergic terminals with other amygdala nuclei exhibiting significantly less cholinergic innervation (Emre et al., 1993).

4.3 | Thalamus

Analysis of the thalamus was limited by lack of an accepted parcellation method for thalamic subnuclei. Nonetheless, our data suggest significant inhomogeneity for [^{18}F]FEOBV binding within the thalamus. The lateral geniculate nuclei exhibited significant [^{18}F]FEOBV binding. Visual inspection suggests less [^{18}F]FEOBV binding in anterior, lateral and some posterior (pulvinar) thalamic subregions. These conclusions are consistent with analysis based on the arbitrary division of the thalamus into eight equivalent octants. Lateral regions exhibited less [^{18}F]FEOBV binding than medial regions and anterior regions less [^{18}F]FEOBV binding than posterior regions. This crude parcellation approach may not adequately assess [^{18}F]FEOBV binding in the pulvinar complex, which likely also exhibits lower [^{18}F]FEOBV binding.

Our results are consistent with the work of Heckers et al. (1992) assessing cholinergic terminal density with ChAT immunohistochemistry in human postmortem specimens. Heckers et al. (1992) documented ChAT immunoreactive fibers throughout the human thalamus with the greatest density of ChAT-immunoreactive fibers in the lateral geniculate nuclei, some intralaminar nuclei, the reunions nucleus, the anterodorsal nucleus, the reticular nucleus, and some portions of the mediodorsal nucleus. Lowest density of ChAT-immunoreactive fibers was seen in the pulvinar and medial geniculate nuclei. As Heckers et al. (1992) point out the human subregional distribution of thalamic cholinergic terminals is likely distinct from that found in the limited number of other species studied (Fitzpatrick et al., 1989; Levey et al., 1987).

The major cholinergic innervation of thalamus originates in the PPN-LDT complex with some contribution from the basal forebrain. PPN-LDT cholinergic efferent projections generally ramify widely and innervate several target regions (Mena-Segovia & Bolam, 2017), though Holmstrand and Sesack (2011) suggest some specialization of cholinergic PPN-LDT afferents targeting the anterior thalamus. In

humans, basal forebrain cholinergic afferents probably innervate more anterior and medial thalamic nuclei, including the central medial and central lateral nuclei, and portions of the mediodorsal nucleus (Heckers et al., 1992).

Cholinergic afferents to the thalamus are implicated in several important phenomena, notably the regulation of consciousness and sleep, though the abundance of cholinergic terminals and receptors within the thalamus suggests cholinergic neurotransmission may modulate multiple aspects of thalamic function. Recent work, for example, from our group suggests that thalamic cholinergic neurotransmission contributes to “bottom-up” detection of salient sensory cues (Kim, Müller, Bohnen, Sarter, & Lustig, 2017).

4.4 | Cerebellum

Prior work in several species suggests significant cholinergic innervation of some cerebellar regions (Barmack, Baughman, & Eckenstein, 1992; Barmack, Baughman, Eckenstein, & Shojaku, 1992; de Lacalle et al., 1993; Fukushima et al., 2001; Jaarsma et al., 1997; Manaye et al., 1999; Zhang et al., 2016). There is no evidence of cholinergic neurons within the cerebellum in most species studied. Cholinergic terminals were detected throughout the cerebellar cortex, though most studies describe these as relatively sparse in most cerebellar cortical regions. [^{18}F]FEOBV PET is likely to convey a more faithful representation of cerebellar cortical innervation than AChase PET methods, which show uniform and high cerebellar cortical tracer retention. Barmack and colleagues (Barmack, Baughman, & Eckenstein, 1992; Barmack, Baughman, Eckenstein, & Shojaku, 1992) described relatively high levels of cholinergic innervation of some cerebellar cortical regions in rat, rabbit, car, and nonhuman primate brain. These included the uvula-nodulus (lobules 9 and 10), the floccular region, and the anterior vermis (lobules 1 and 2) (Barmack, Baughman, & Eckenstein, 1992; Barmack, Baughman, Eckenstein, & Shojaku, 1992). The predominant source of these terminals appears to be cholinergic neurons of the vestibular complex. Jaarsma et al. (1997) also described cholinergic afferents to the cerebellar cortex from numerous brainstem populations, though MVC cholinergic neurons were felt to be the predominant source of cerebellar cortical afferents. de Lacalle et al. (1993) described a ChAT-immunoreactive subpopulation of cerebellar cortical Golgi interneurons, particularly in the vermis, uvula-nodulus, and flocculus, in human postmortem specimens.

We find uniformly high [^{18}F]FEOBV binding throughout the vermis, different from the patterns described in other mammals. The originating neurons of this extensive cerebellar vermis cholinergic innervation are unknown, though it is possible that it is an extension of the vestibulocerebellar cholinergic innervation documented in other mammals. Alternatively, the pattern of cerebellar [^{18}F]FEOBV binding may reflect the distribution of cholinergic Golgi interneurons described by de Lacalle et al. (1993). The vestibular system plays a critical role in the maintenance of normal upright posture and gait, as does the cerebellar vermis. A plausible speculation is that extended vestibular cholinergic innervation of the cerebellar vermis is a correlate of bipedal locomotion in humans. Seidel et al. (2015) document α -synuclein aggregate pathology in the MVC nuclei of postmortem specimens from individuals with Parkinson disease and Lewy body

dementia. It is possible that vestibular dysfunction contributes to the dopamine replacement therapy refractory gait and balance deficits of advanced Parkinson disease.

Another previously documented site of cholinergic innervation of the cerebellum is the deep cerebellar nuclei. Prior tract-tracing and functional studies in rodents indicate projections from the PPN-LDT complex to the deep cerebellar nuclei with MRI tractography studies supporting the existence of this projection in humans (Aravamuthan, Muthusamy, Stein, Aziz, & Johansen-Berg, 2007; Vitale et al., 2016). These terminals are presumably too sparse to be detected by [^{18}F]FEOBV PET.

4.5 | Brainstem

Cholinergic neurons within the brainstem include oculomotor (CrN III, IV, and VI nuclei), motor (motor nucleus of CrN V, and CrN VII, CrN X, XI, and CrN XII nuclei), and autonomic nuclei (Vagal Nucleus), and some MVC neurons. Most of these nuclei are beyond the resolution of PET imaging. The largest collection of brainstem cholinergic neurons lies within the PPN-LDT complex (Mesulam et al., 1983, Chapter 5 and 6). In immunohistochemical studies of postmortem human specimens, Mesulam et al. (1989) described the PPN-LDT complex as stretching from the dorsal mid-mesencephalon to dorsal mid-pons. The distribution of cholinergic perikarya did not observe specific nuclear borders nor was it delimited by fiber tracts. Cholinergic perikarya were distributed at varying densities throughout this volume of the brainstem. Similar results were obtained by Manaye et al. (1999). In rodent PPN-LDT, there is a rostrocaudal gradient of cholinergic perikarya density with the highest density of these neurons in the caudal PPN-LDT complex (Mena-Segovia & Bolam, 2017). The distribution of cholinergic perikarya described in humans by Mesulam et al. (1989) coincides well with the distribution of relatively high [^{18}F]FEOBV binding we find spanning the dorsal mesopontine junction. This area of relatively high brainstem [^{18}F]FEOBV binding may also include the cholinergic parabigeminal nucleus (Mesulam et al., 1983, Chapter 8), adjacent and lateral to the PPN-LDT complex in the upper pons.

We found significant [^{18}F]FEOBV binding throughout the brainstem, most likely the binding to the terminals of PPN-LDT neurons that innervate multiple targets throughout the brainstem (Woolf & Butcher, 1989). While our analysis is limited by the resolution of PET, prior studies in other species do not describe marked inhomogeneity of brainstem cholinergic terminals. It was possible to tentatively identify what might be a column of relatively increased [^{18}F]FEOBV binding in the dorsal caudal brainstem surrounding the aqueduct (Figures 1 and Figure 5).

4.6 | Aging effects

Our results indicate significant and regionally specific declines in [^{18}F]FEOBV binding. Striatal complex changes are consistent with age-related declines in striatal cholinergic interneuron terminal density. There was a suggestion of reduced thalamic [^{18}F]FEOBV binding, consistent with age-related decrease in PPN-LDT complex cholinergic terminals. Ransmayr et al. (2000) described age-related loss of PPN

neurons in humans. Zhang, Sampogna, Morales, & Chase (2005) studied PPN-LDT neurons in aged cats. There was no evidence of PPN-LDT cholinergic perikarya loss but there was evidence of neuronal atrophy and dendritic simplification. Prior work suggests age-related changes in BF neurons. MRI morphometry studies indicate age-related loss of BF nuclear volumes (Grothe, Heinsen, & Teipel, 2012; Hanyu et al., 2002). These results are consistent with our data suggesting age-related loss of BF corticopetal terminals. Our data suggest that this is not a uniform process as we found cortical regions (primary sensorimotor cortex, anterior cingulate cortices) with significant declines in [^{18}F]FEOBV binding and others with little or no age-related change. As subpopulations of BF neurons are thought to project to relatively restricted cortical regions (Gielow & Zaborszky, 2017), our results suggest inhomogeneous age-related changes within the BF complex. Prior SPECT studies of human VAcHT distribution also suggested age-related decline in BF corticopetal terminals but lacked the precision to resolve changes in individual neocortical regions (Kuhl et al., 1996).

4.7 | General conclusion

[^{18}F]FEOBV PET delineates regional cholinergic terminals well in human brains. The general pattern of [^{18}F]FEOBV binding is highly consistent with the known organization of major cholinergic systems in mammalian brain. Our results indicate distinctive organization of cholinergic terminals in the human neocortex, cerebellar cortex, and the human thalamus. Our results indicate the presence of age-related and region-specific changes in cholinergic terminal density. [^{18}F]FEOBV PET is likely to be a useful method for studying disease states, including several neurodegenerative disorders and psychiatric disorders.

ACKNOWLEDGMENTS

The authors thank our research participants and the technical staff of the University of Michigan PET Center. This study was supported by P01 NS015655, P50 NS091856, R21 NS088302, and the Michael J. Fox Foundation.

ORCID

Roger L. Albin  <https://orcid.org/0000-0002-0629-608X>

REFERENCES

- Aghourian, M., Legault-Denis, C., Soucy, J. P., Rosa-Neto, P., Gauthier, S., Kostikov, A., ... Bédard, M. A. (2017). Quantification of brain cholinergic denervation in Alzheimer's disease using PET imaging with [^{18}F]FEOBV. *Molecular Psychiatry*, 22, 1531–1538.
- Albin, R. L., Koeppe, R. A., Bohnen, N. I., Wernette, K., Kilbourn, M. A., & Frey, K. A. (2008). Spared caudal brainstem SERT binding in early Parkinson's disease. *Journal of Cerebral Blood Flow and Metabolism*, 28, 441–444.
- Albin, R. L., Minderovic, C., & Koeppe, R. A. (2017). Normal striatal vesicular acetylcholine transporter expression in Tourette syndrome. *eNeuro*, 4, 017817.
- Albin, R. L., Morgan, M. M., Higgins, D. S., & Frey, K. A. (1994). Autoradiographic quantification of muscarinic cholinergic synaptic markers in bat, shrew, and rat brain. *Neurochemical Research*, 19, 581–589.

- Anthenelli, R. M., Benowitz, N. L., West, R., St. Aubin, L., McRae, T., Lawrence, D., ... Ewins, A. E. (2016). Neuropsychiatric safety and efficacy of varenicline, bupropion, and nicotine patch in smokers with and without psychiatric disorders (EAGLES): A double-blind, randomised, placebo-controlled clinical trial. *Lancet*, *387*, 2507–2520.
- Aoki, S., Liu, A. W., Zucca, A., Zucca, S., & Wickens, J. R. (2015). Role of striatal cholinergic interneurons in set-shifting in the rat. *Journal of Neuroscience*, *35*, 9424–9431.
- Aravamuthan, B. R., Muthusamy, K. A., Stein, J. F., Aziz, T. Z., & Johansen-Berg, H. (2007). Topography of cortical and subcortical connections of the human pedunclopontine and subthalamic nuclei. *NeuroImage*, *37*, 694–705.
- Arvidsson, U., Riedel, M., Elde, R., & Meister, B. (1997). Vesicular acetylcholine transporter (VACHT) protein: A novel and unique marker for cholinergic neurons in the central and peripheral nervous systems. *Journal of Comparative Neurology*, *378*, 454–467.
- Ballinger, E. C., Ananth, M., Talmage, D. A., & Role, L. W. (2016). Basal forebrain cholinergic circuits and signaling in cognition and cognitive decline. *Neuron*, *91*, 1199–1218.
- Barmack, N. H., Baughman, R. W., & Eckenstein, F. P. (1992). Cholinergic innervation of the cerebellum of rat, rabbit, cat, and monkey as revealed by choline acetyltransferase activity and immunohistochemistry. *Journal of Comparative Neurology*, *317*, 233–249.
- Barmack, N. H., Baughman, R. W., Eckenstein, F. P., & Shojaku, H. (1992). Secondary vestibular cholinergic projection to the cerebellum of rabbit and rat as revealed by choline acetyltransferase immunohistochemistry, retrograde and orthograde tracers. *Journal of Comparative Neurology*, *317*, 250–270.
- Bernácer, J., Prensa, L., & Giménez-Amaya, J. M. (2007). Cholinergic interneurons are differentially distributed in the human striatum. *PLoS One*, *2*, e1174.
- Bohnen, N. I., Albin, R. L., Koeppe, R. A., Wernette, K. A., Kilbourn, M. R., Minoshima, S., & Frey, K. A. (2006). Positron emission tomography of monoaminergic vesicular binding in aging and Parkinson disease. *Journal of Cerebral Blood Flow and Metabolism*, *26*, 1198–1212.
- Bohnen, N. I., Müller, M. L., Kotagal, V., Koeppe, R. A., Kilbourn, M. R., Gilman, S., ... Frey, K. A. (2012). Heterogeneity of cholinergic denervation in Parkinson's disease without dementia. *Journal of Cerebral Blood Flow and Metabolism*, *32*, 1609–1617.
- Chung, K. A., Lobb, B. M., Nutt, J. G., & Horak, F. B. (2010). Effects of a central cholinesterase inhibitor on reducing falls in Parkinson disease. *Neurology*, *75*, 1263–1269.
- Dautan, D., Hacıoğlu Bay, H., Bolam, J. P., Gerdjikov, T. V., & Mena-Segovia, J. (2016). Extrinsic sources of cholinergic innervation of the striatal complex: A whole-brain mapping analysis. *Frontiers in Neuroanatomy*, *10*, 1.
- Dautan, D., Huerta-Ocampo, I., Witten, I. B., Deisseroth, K., Bolam, J. P., Gerdjikov, T., & Mena-Segovia, J. (2014). A major external source of cholinergic innervation of the striatum and nucleus accumbens originates in the brainstem. *Journal of Neuroscience*, *34*, 4509–4518.
- de Lacalle, S., Hersh, L. B., & Saper, C. B. (1993). Cholinergic innervation of the human cerebellum. *Journal of Comparative Neurology*, *328*, 364–376.
- de Lacalle, S., Lim, C., Sobreviela, T., Mufson, E. J., Hersh, L. B., & Saper, C. B. (1994). Cholinergic innervation in the human hippocampal formation including the entorhinal cortex. *Journal of Comparative Neurology*, *345*, 321–344.
- Deffains, M., & Bergman, H. (2015). Striatal cholinergic interneurons and cortico-striatal synaptic plasticity in health and disease. *Movement Disorders*, *30*, 1014–1025.
- DeKosky, S. T., Harbaugh, R. E., Schmitt, F. A., Bakay, R. A., Chui, H. C., Knopman, D. S., ... Markesbery, W. R. (1992). Cortical biopsy in Alzheimer's disease: Diagnostic accuracy and neurochemical, neuropathological, and cognitive correlations. Intraventricular Bethanecol Study Group. *Annals of Neurology*, *32*, 625–632.
- Eiden, L. E. (1998). The cholinergic gene locus. *Journal of Neurochemistry*, *70*, 2227–2240.
- Emre, M., Heckers, S., Mash, D. C., Geula, C., & Mesulam, M. M. (1993). Cholinergic innervation of the amygdaloid complex in the human brain and its alterations in old age and Alzheimer's disease. *Journal of Comparative Neurology*, *336*, 117–134.
- Fitzpatrick, D., Diamond, I. T., & Raczkowski, D. (1989). Cholinergic and monoaminergic innervation of the cat's thalamus: Comparison of the lateral geniculate nucleus with other principal sensory nuclei. *Journal of Comparative Neurology*, *288*, 647–675.
- Fukushima, M., Kitahara, T., Takeda, N., Saika, T., Uno, A., & Kubo, T. (2001). Role of cholinergic mossy fibers in medial vestibular and prepositus hypoglossal nuclei in vestibular compensation. *Neuroscience*, *102*, 159–166.
- Gielow, M. R., & Zaborszky, L. (2017). The input-output relationship of the cholinergic basal forebrain. *Cell Reports*, *18*, 1817–1830.
- Gilman, S., Koeppe, R. A., Nan, B., Wang, C. N., Wang, X., Junck, L., ... Bhaumik, A. (2010). Cerebral cortical and subcortical cholinergic deficits in parkinsonian syndromes. *Neurology*, *74*, 1416–1423.
- Gilmor, M. L., Erickson, J. D., Varoqui, H., Hersh, L. B., Bennett, D. A., Cochran, E. J., ... Levey, A. I. (1999). Preservation of nucleus basalis neurons containing choline acetyltransferase and the vesicular acetylcholine transporter in the elderly with mild cognitive impairment and early Alzheimer's disease. *Journal of Comparative Neurology*, *411*, 693–704.
- Gilmor, M. L., Nash, N. R., Roghani, A., Edwards, R. H., Yi, H., Hersch, S. M., & Levey, A. I. (1996). Expression of the putative vesicular acetylcholine transporter in rat brain and localization in cholinergic synaptic vesicles. *Journal of Neuroscience*, *16*, 2179–2190.
- Gonzales, K. K., & Smith, Y. (2015). Cholinergic interneurons in the dorsal and ventral striatum: Anatomical and functional considerations in normal and diseased conditions. *Annals of the New York Academy of Sciences*, *1349*, 1–45.
- Greenfield, S. A. (1991). A noncholinergic action of acetylcholinesterase (AChE) in the brain: From neuronal secretion to the generation of movement. *Cellular and Molecular Neurobiology*, *11*, 55–77.
- Grothe, M., Heinsen, H., & Teipel, S. J. (2012). Atrophy of the cholinergic basal forebrain over the adult age range and in early stages of Alzheimer's disease. *Biological Psychiatry*, *71*, 805–813.
- Gut, N. K., & Winn, P. (2016). The pedunclopontine tegmental nucleus—a functional hypothesis from the comparative literature. *Movement Disorders*, *31*, 615–624.
- Hanyu, H., Asano, T., Sakurai, H., Tanaka, Y., Takasaki, M., & Abe, K. (2002). MR analysis of the substantia innominata in normal aging, Alzheimer disease, and other types of dementia. *American Journal of Neuroradiology*, *23*, 27–32.
- Hasselmo, M. E., & Sarter, M. (2011). Modes and models of forebrain cholinergic neuromodulation of cognition. *Neuropsychopharmacology*, *36*, 52–73.
- Heckers, S., Geula, C., & Mesulam, M. M. (1992). Cholinergic innervation of the human thalamus: Dual origin and differential nuclear distribution. *Journal of Comparative Neurology*, *325*, 68–82.
- Henderson, E. J., Lord, S. R., Brodie, M. A., Gaunt, D. M., Lawrence, A. D., Close, J. C., ... Ben-Shlomo, Y. (2016). Rivastigmine for gait stability in patients with Parkinson's disease (ReSPonD): A randomised, double-blind, placebo-controlled, phase 2 trial. *Lancet Neurology*, *15*, 249–258.
- Hirsch, E. C., Graybiel, A. M., Duyckaerts, C., & Javoy-Agid, F. (1987). Neuronal loss in the pedunclopontine tegmental nucleus in Parkinson disease and in progressive supranuclear palsy. *Proceedings of the National Academy of Sciences of the United States of America*, *84*, 5976–5980.
- Holmstrand, E. C., & Sesack, S. R. (2011). Projections from the rat pedunclopontine and laterodorsal tegmental nuclei to the anterior thalamus and ventral tegmental area arise from largely separate populations of neurons. *Brain Structure and Function*, *216*, 331–345.
- Ichikawa, T., Ajiki, K., Matsuura, J., & Misawa, H. (1997). Localization of two cholinergic markers, choline acetyltransferase and vesicular acetylcholine transporter in the central nervous system of the rat: In situ hybridization histochemistry and immunohistochemistry. *Journal of Chemical Neuroanatomy*, *13*, 23–39.
- Iyo, M., Namba, H., Fukushi, K., Shinotoh, H., Nagatsuka, S., Sahara, T., ... Irie, T. (1997). Measurement of acetylcholinesterase by positron emission tomography in the brains of healthy controls and patients with Alzheimer's disease. *Lancet*, *349*, 1805–1809.
- Jaarsma, D., Ruigrok, T. J., Caffé, R., Cozzari, C., Levey, A. I., Mugnaini, E., & Voogd, J. (1997). Cholinergic innervation and receptors in the cerebellum. *Progress in Brain Research*, *114*, 67–96.

- Janickova, H., Rosborough, K., Al-Onaizi, M., Kljakic, O., Guzman, M. S., Gros, R., ... Prado, V. F. (2017). Deletion of the vesicular acetylcholine transporter from pedunculopontine/laterodorsal tegmental neurons modifies gait. *Journal of Neurochemistry*, *140*, 787–798.
- Kim, K., Müller, M. L. T. M., Bohnen, N. I., Sarter, M., & Lustig, C. (2017). Thalamic cholinergic innervation makes a specific bottom-up contribution to signal detection: Evidence from Parkinson's disease patients with defined cholinergic losses. *NeuroImage*, *149*, 295–304.
- Kucinski, A., de Jong, I. E., & Sarter, M. (2017). Reducing falls in Parkinson's disease: Interactions between donepezil and the 5-HT₆ receptor antagonist idalopirdine on falls in a rat model of impaired cognitive control of complex movements. *European Journal of Neuroscience*, *45*, 217–231.
- Kuhl, D. E., Koeppe, R. A., Fessler, J. A., Minoshima, S., Ackermann, R. J., Carey, J. E., ... Wieland, D. M. (1994). In vivo mapping of cholinergic neurons in the human brain using SPECT and IBVM. *Journal of Nuclear Medicine*, *35*, 405–410.
- Kuhl, D. E., Koeppe, R. A., Minoshima, S., Snyder, S. E., Ficaró, E. P., Foster, N. L., ... Kilbourn, M. R. (1999). In vivo mapping of cerebral acetylcholinesterase activity in aging and Alzheimer's disease. *Neurology*, *52*, 691–699.
- Kuhl, D. E., Minoshima, S., Fessler, J. A., Frey, K. A., Foster, N. L., Ficaró, E. P., ... Koeppe, R. A. (1996). In vivo mapping of cholinergic terminals in normal aging, Alzheimer's disease, and Parkinson's disease. *Annals of Neurology*, *40*, 399–410.
- Kus, L., Borys, E., Ping Chu, Y., Ferguson, S. M., Blakely, R. D., Emborg, M. E., ... Mufson, E. J. (2003). Distribution of high affinity choline transporter immunoreactivity in the primate central nervous system. *Journal of Comparative Neurology*, *463*, 341–357.
- Lamare, F., Mazere, J., Attila, M., Mayo, W., De Clermont-Gallerande, H., Meissner, W., ... Allard, M. (2013). Improvement of in vivo quantification of [123I]-Iodobenzovesamicol in single-photon emission computed tomography/computed tomography using anatomic image to brain atlas nonrigid registration. *Molecular Imaging*, *12*, 288–299.
- Laplante, F., Lappi, D. A., & Sullivan, R. M. (2011). Cholinergic depletion in the nucleus accumbens: Effects on amphetamine response and sensorimotor gating. *Progress in Neuro-Psychopharmacology & Biological Psychiatry*, *35*, 501–509.
- Lecumberri, A., Lopez-Janeiro, A., Corral-Domenge, C., & Bernacer, J. (2018). Neuronal density and proportion of interneurons in the associative, sensorimotor and limbic human striatum. *Brain Structure & Function*, *223*, 1615–1625.
- Levey, A. I., Hallanger, A. E., & Wainer, B. H. (1987). Choline acetyltransferase immunoreactivity in the rat thalamus. *Journal of Comparative Neurology*, *257*, 317–332.
- Li, Z., Yu, Z., Zhang, J., Wang, J., Sun, C., Wang, P., & Zhang, J. (2015). Impact of Rivastigmine on cognitive dysfunction and falling in Parkinson's disease patients. *European Neurology*, *74*, 86–91.
- Mahady, L. J., Perez, S. E., Emerich, D. F., Wahlberg, L. U., & Mufson, E. J. (2017). Cholinergic profiles in the Goettingen miniature pig (*Sus scrofa domestica*) brain. *Journal of Comparative Neurology*, *525*, 553–573.
- Manaye, K. F., Zweig, R., Wu, D., Hersh, L. B., De Lacalle, S., Saper, C. B., & German, D. C. (1999). Quantification of cholinergic and select non-cholinergic mesopontine neuronal populations in the human brain. *Neuroscience*, *89*, 759–770.
- Martos, Y. V., Braz, B. Y., Beccaria, J. P., Murer, M. G., & Belforte, J. E. (2017). Compulsive social behavior emerges after selective ablation of striatal cholinergic interneurons. *Journal of Neuroscience*, *37*, 2849–2858.
- Mena-Segovia, J., & Bolam, J. P. (2017). Rethinking the Pedunculopontine nucleus: From cellular organization to function. *Neuron*, *94*, 7–18.
- Mesulam, M. M. (2004). The cholinergic innervation of the human cerebral cortex. *Progress in Brain Research*, *145*, 67–78.
- Mesulam, M. M. (2013). Cholinergic circuitry of the human nucleus basalis and its fate in Alzheimer's disease. *Journal of Comparative Neurology*, *521*, 4124–4144.
- Mesulam, M. M., & Geula, C. (1988). Nucleus basalis (Ch4) and cortical cholinergic innervation in the human brain: Observations based on the distribution of acetylcholinesterase and choline acetyltransferase. *Journal of Comparative Neurology*, *275*, 216–240.
- Mesulam, M. M., Geula, C., Bothwell, M. A., & Hersh, L. B. (1989). Human reticular formation: Cholinergic neurons of the pedunculopontine and laterodorsal tegmental nuclei and some cytochemical comparisons to forebrain cholinergic neurons. *Journal of Comparative Neurology*, *283*, 611–633.
- Mesulam, M. M., Hersh, L. B., Mash, D. C., & Geula, C. (1992). Differential cholinergic innervation within functional subdivisions of the human cerebral cortex: A choline acetyltransferase study. *Journal of Comparative Neurology*, *318*, 316–328.
- Mesulam, M. M., Mash, D., Hersh, L., Bothwell, M., & Geula, C. (1992). Cholinergic innervation of the human striatum, globus pallidus, subthalamic nucleus, substantia nigra, and red nucleus. *Journal of Comparative Neurology*, *323*, 252–268.
- Mesulam, M. M., Mufson, E. J., Wainer, B. H., & Levey, A. I. (1983). Central cholinergic pathways in the rat: An overview based on an alternative nomenclature (Ch1-Ch6). *Neuroscience*, *10*, 1185–1201.
- Mufson, E. J., Ginsberg, S. D., Ikonovic, M. D., & DeKosky, S. T. (2003). Human cholinergic basal forebrain: Chemoanatomy and neurologic dysfunction. *Journal of Chemical Neuroanatomy*, *26*, 233–242.
- Mulholland, G. K., Wieland, D. M., Kilbourn, M. R., Frey, K. A., Sherman, P. S., Carey, J. E., & Kuhl, D. E. (1998). [18F]fluoroethoxybenzovesamicol, a PET radiotracer for the vesicular acetylcholine transporter and cholinergic synapses. *Synapse*, *30*, 263–274.
- Pappas, S. S., Darr, K., Holley, S. M., Cepeda, C., Mabrouk, O. S., Wong, J. M., ... Dauer, W. T. (2015). Forebrain deletion of the dystonia protein torsinA causes dystonic-like movements and loss of striatal cholinergic neurons. *eLife*, *4*, e08352.
- Petrou, M., Frey, K. A., Kilbourn, M. R., Scott, P. J., Raffel, D. M., Bohnen, N. I., ... Koeppe, R. A. (2014). In vivo imaging of human cholinergic nerve terminals with (–)-5-(18F)-fluoroethoxybenzovesamicol: Biodistribution, dosimetry, and tracer kinetic analyses. *Journal of Nuclear Medicine*, *55*, 396–404.
- Pienaar, I. S., Vernon, A., & Winn, P. (2016). The cellular diversity of the Pedunculopontine nucleus: Relevance to behavior in health and aspects of Parkinson's disease. *The Neuroscientist*, *23*, 415–431.
- Prado, V. F., Janickova, H., Al-Onaizi, M. A., & Prado, M. A. (2017). Cholinergic circuits in cognitive flexibility. *Neuroscience*, *345*, 130–141.
- Prado, V. F., Roy, A., Kolisnyk, B., Gros, R., & Prado, M. A. (2013). Regulation of cholinergic activity by the vesicular acetylcholine transporter. *Biochemical Journal*, *450*, 265–274.
- Ransmayr, G., Faucheux, B., Nowakowski, C., Kubis, N., Federspiel, S., Kaufmann, W., ... Hirsch, E. C. (2000). Age-related changes of neuronal counts in the human pedunculopontine nucleus. *Neuroscience Letters*, *288*, 195–198.
- Roghani, A., Shirzadi, A., Butcher, L. L., & Edwards, R. H. (1998). Distribution of the vesicular transporter for acetylcholine in the rat central nervous system. *Neuroscience*, *82*, 1195–1212.
- Schäfer, M. K., Eiden, L. E., & Weihe, E. (1998). Cholinergic neurons and terminal fields revealed by immunohistochemistry for the vesicular acetylcholine transporter. I. Central nervous system. *Neuroscience*, *84*, 331–359.
- Schafer, M. K., Weihe, E., Erickson, J. D., & Eiden, L. E. (1995). Human and monkey cholinergic neurons visualized in paraffin-embedded tissues by immunoreactivity for VACht, the vesicular acetylcholine transporter. *Journal of Molecular Neuroscience*, *6*, 225–235.
- Schliebs, R., & Arendt, T. (2011). The cholinergic system in aging and neuronal degeneration. *Behavioural Brain Research*, *221*, 555–563.
- Seidel, K., Mahlke, J., Siswanto, S., Krüger, R., Heinsen, H., Auburger, G., ... Rüb, U. (2015). The brainstem pathologies of Parkinson's disease and dementia with Lewy bodies. *Brain Pathology*, *25*, 121–135.
- Shao, X., Hoareau, R., Hockley, B. G., Tluczek, L. J., Henderson, B. D., Padgett, H. C., & Scott, P. J. (2011). Highlighting the versatility of the Tracerlab synthesis modules. Part 1: Fully automated production of [F] labelled radiopharmaceuticals using a Tracerlab FX(FN). *Journal of Labelled Compounds & Radiopharmaceuticals*, *54*, 292–307.
- Snyder, S. E., Gunupudi, N., Sherman, P. S., Butch, E. R., Skaddan, M. B., Kilbourn, M. R., ... Kuhl, D. E. (2001). Radiolabeled cholinesterase substrates: in vitro methods for determining structure-activity relationships and identification of a positron emission tomography radiopharmaceutical for in vivo measurement of butyrylcholinesterase activity. *Journal of Cerebral Blood Flow & Metabolism*, *21*, 132–143.
- Tanimura, A., Pancani, T., Lim, S. A. O., Tubert, C., Melendez, A. E., Shen, W., & Surmeier, D. J. (2017). Striatal cholinergic interneurons and Parkinson's disease. *European Journal of Neuroscience*, *47*, 1148–1158.

- Vitale, F., Mattei, C., Capozzo, A., Pietrantonì, I., Mazzone, P., & Scarnati, E. (2016). Cholinergic excitation from the pedunculo-pontine tegmental nucleus to the dentate nucleus in the rat. *Neuroscience*, *317*, 12–22.
- Woolf, N. J. (1991). Cholinergic systems in mammalian brain and spinal cord. *Progress in Neurobiology*, *37*, 475–524.
- Woolf, N. J., & Butcher, L. L. (1985). Cholinergic systems in the rat brain: II. Projections to the interpeduncular nucleus. *Brain Research Bulletin*, *14*, 63–83.
- Woolf, N. J., & Butcher, L. L. (1986). Cholinergic systems in the rat brain: III. Projections from the pontomesencephalic tegmentum to the thalamus, tectum, basal ganglia, and basal forebrain. *Brain Research Bulletin*, *16*, 603–637.
- Woolf, N. J., & Butcher, L. L. (1989). Cholinergic systems in the rat brain: IV. Descending projections of the pontomesencephalic tegmentum. *Brain Research Bulletin*, *23*, 519–540.
- Woolf, N. J., Eckenstein, F., & Butcher, L. L. (1984). Cholinergic systems in the rat brain: I. projections to the limbic telencephalon. *Brain Research Bulletin*, *13*, 751–784.
- Zhang, J. H., Sampogna, S., Morales, F. R., & Chase, M. H. (2005). Age-related changes in cholinergic neurons in the laterodorsal and the pedunculo-pontine tegmental nuclei of cats: a combined light and electron microscopic study. *Brain Research*, *1052*, 47–55.
- Zhang, C., Zhou, P., & Yuan, T. (2016). The cholinergic system in the cerebellum: From structure to function. *Reviews in the Neurosciences*, *27*, 769–776.

How to cite this article: Albin RL, Bohnen NI, Muller MLTM, et al. Regional vesicular acetylcholine transporter distribution in human brain: A [¹⁸F]fluoroethoxybenzovesamicol positron emission tomography study. *J Comp Neurol*. 2018;526: 2884–2897. <https://doi.org/10.1002/cne.24541>